Received 3 March 2025; revised 26 March 2025; accepted 4 April 2025. Date of publication 7 April 2025; date of current version 12 August 2025.

Digital Object Identifier 10.1109/OJAP.2025.3558671

Experimental Evaluation of Enhanced Antenna Switching for CFO Mitigation in DoA Estimation

ALEŠ SIMONČIČ [1,2] (Student Member, IEEE), KE GUAN [1,3] (Senior Member, IEEE), GREGA MORANO [1,2] (Graduate Student Member, IEEE), ALEŠ ŠVIGELJ [1,2] (Senior Member, IEEE), ANDREJ HROVAT [1,2] (Senior Member, IEEE), TEODORA KOCEVSKA [1] (Member, IEEE), AND TOMAŽ JAVORNIK [1,2] (Member, IEEE)

[1]Department of Communication Systems, Jožef Stefan Institute, 1000 Ljubljana, Slovenia
[2]Jožef Stefan International Postgraduate School, 1000 Ljubljana, Slovenia
[3]State Key Laboratory of Advanced Rail Autonomous Operation and the School of Electronic and Information Engineering, Beijing Jiaotong University, 100044 Beijing, China

CORRESPONDING AUTHOR: A. SIMONČIČ (e-mail: ales.simoncic@ijs.si)

This work was supported by the Slovenian Research and Innovation Agency (ARIS) under Grant PR-12348, Grant J2-4461, Grant J2-3048, and Grant P2-0016.

ABSTRACT Direction-of-arrival (DoA) estimation in the Internet of Things (IoT) and embedded devices is typically performed using single-RF chain systems and antenna switching using time-division multiplexing. The accuracy of the DoA estimation is reduced due to the additional phase shifts between the samples on the antenna elements caused by the carrier frequency offset (CFO). We propose to use optimized antenna switching patterns (ASPs) to mitigate the effect of CFO on accuracy in DoA estimation using a multiple signal classification (MUSIC) algorithm. We evaluated two switching methods referred to as *EvenCFO-SP* and *Mirror-SP* with simulations and confirmed the validity with measurements. Performance is analyzed and compared with a standard sequential sampling (SS) method. Uniform linear and circular array configurations are considered to evaluate the impact of the noise and the CFO value on estimation accuracy. The results show that the optimized ASPs outperform the SS method, with lower performance gain at small signal-to-noise ratios. The ASP sensitivity to the CFO value is studied, and the frequency bounds within which the optimized ASPs maintain high estimation accuracy are identified. A coarse CFO correction, effective for frequency estimation errors within the kHz range, extends the frequency bounds. Compared to a fine calibration, this reduces computational requirements, making it a viable option for embedded and IoT devices with limited hardware resources.

INDEX TERMS Antenna switching pattern (ASP), carrier frequency offset (CFO), direction-of-arrival (DoA), Internet of Things (IoT), MUSIC, noise, single-RF chain, switched array, uniform circular array (UCA), uniform linear array (ULA).

I. INTRODUCTION

LOCALIZATION functionality within Internet of Things (IoT) devices is increasingly important for emerging industries, precision agriculture, autonomous transportation, environmental monitoring, asset tracking, disaster response, wearable technology, smart homes, and more [1]. Accurate location information considerably extends the benefits of IoT systems [2]. Among localization methods, the estimation of the direction of arrival (DoA) is favored in practice due to its high precision without the need for precise time synchronization between devices [3], [4]. However, the computational and power limitations of devices within massive IoT networks present challenges in achieving a precise DoA estimation, creating a need for solutions that meet strict accuracy requirements while considering limited resources.

Various IoT communication standards have integrated DoA estimation functionality. High-accuracy indoor positioning is enabled in Bluetooth Low Energy (BLE) with its angle-of-arrival (AoA) / angle-of-departure (AoD) functionality [5]. Accurate localization in dense IoT networks in industrial environments is possible with DoA estimation within the 6TiSCH standard [6].

Single-RF chain systems are common in IoT devices due to cost constraints, where samples for DoA estimation are acquired by switching antenna elements using time-division multiplexing [7]. The accuracy of DoA estimation is reduced by the presence of carrier frequency offset (CFO) and antenna switching, which introduce additional phase shifts at the antenna elements. The CFO is caused mainly by the low-cost design with low-accuracy crystal oscillators and is additionally affected by temperature variations, component aging, and power stability fluctuations.

Estimation and correction methods are conventionally used to address the CFO effect on DoA estimation. Fine estimation leads to an unacceptably high computational overhead for resource-constrained IoT and embedded devices, affecting real-time responsiveness. Therefore, more computationally efficient methods are required. This study proposes to exploit the signal sampling order of antenna elements referred to as the antenna switching pattern (ASP). ASP is represented as an ordered sequence of antenna element indices that determines the sampling order of the signal across the antenna elements.

Sequential sampling (SS) is typically used with switching based on round-robin (RR), where antenna elements are activated sequentially in their spatial order, looping back to the first antenna element after completing a full cycle. In this work, we propose to optimize the ASP for reducing the systematic error in DoA estimation with the multiple signal classification (MUSIC) algorithm by considering the phase shifts at the antenna elements as counter-weighed weights and compensating the systematic error using the reverse order ASP configuration. The main contributions of the paper are summarized as follows:

- Formulation of the ASP optimization for mitigating the CFO impact on DoA estimation and ASP design;
- Performance evaluation of the optimized ASPs for uniform linear arrays (ULAs) and uniform circular arrays (UCAs) compared to a baseline SS approach;
- Analysis of the impact of noise and CFO on the effectiveness of the optimized ASPs;
- Experimental validation of DoA estimation with optimized antenna switching for CFO mitigation using measurements.

The remainder of the paper is organized as follows. After the introduction, the related work is summarized in Section II. Section III formalizes the antenna switching pattern optimization. The ASP performance evaluation with simulations is discussed in Section IV. Section V describes the experimental validation. Finally, the findings and future directions are summarized in Section VI.

II. RELATED WORK

Phase correction after CFO estimation is a conventional technique to reduce DoA estimation errors. A single antenna has to be used to obtain the samples because phase shifts exist for multiple antenna elements due to the different propagation lengths of the signal. For example, in the standardized direction estimation in BLE, a preamble with constant tone extension provides eight IQ samples acquired with a reference antenna. The CFO can be estimated with algorithms such as linear regression, the fast Fourier transform (FFT), the Moose algorithm, and MUSIC, which differ in the trade-off between accuracy and computational complexity [6], [8], [9]. High-precision algorithms such as MUSIC are accurate, computationally intensive, and may exceed the device's capabilities. Simpler and computationally lighter methods, such as linear regression, cannot provide the precision required for high-resolution DoA applications. Maximizing the samples over a long period, as in the return-to-first ASP, where the switching is based on returning to a reference antenna after sampling, results in more accurate CFO estimation while increasing the transmission time, power consumption, and likelihood of interference. Using samples for CFO estimation from sample slots longer than the acquisition time is another approach suggested for improving accuracy [6]. The accuracy of DoA estimation can be improved by exploiting the ASP. In [10], authors analyzed how the number of samples acquired on each antenna element before switching and the different ASPs affect the Cramér-Rao bound (CRB) for the estimation of sinusoidal parameters and the estimation of DoA. Through an exhaustive search, they identified the ASP that provided the lowest CRB and introduced a *Mirrored Rotation* ASP and showed that these two ASPs improve the performance over SS ASP.

Techniques developed for Doppler shift mitigation in frequency-modulated continuous wave (FMCW) radar systems can be adapted and applied to combat the CFO effect on DoA estimation accuracy due to the similarity of the problem. One of the main issues is the additional phase shift between antenna switching times correlated to the phase shifts caused by DoA impinging on the ULA for moving targets. An ASP was designed for the ULA configuration and a simple mathematical operation was applied on the first three antenna elements of the ASP to remove the effect of velocity on DoA estimation [11]. To eliminate phase shifts caused by motion without velocity estimation and correction, a double-time switching scheme based on reference samples equal to the number of antenna elements was proposed, where reference values are first acquired from a single antenna element, then the antenna elements are switched in sequential pattern, and the acquired phases are subtracted from the references [12]. Another approach without estimation-calibration procedure was proposed in [13] that introduces two ASPs where the sign of velocity-induced phase shifts alternates between the indices in the ASP, which produces high-frequency, windowed, sinusoidal-like phase shifts that minimally affect slope estimation and effectively reduce ghost targets. Switching performed in a single frequency modulation period considering randomized ASP was studied to evaluate how the different random realizations of ASP affect the resolution and sidelobe levels based on the analysis of the ambiguity function showing

that lowest sidelobes and resolution can be achieved with a random permutation of antenna element indexes varied for each modulation cycle [14].

Optimizing the ASP was applied in channel-sounding applications for extending the Doppler frequency estimation range for switched arrays with SS ASP, since a trade-off exists between an accurate AoA/AoD estimation, where more antenna elements result in better performance, and the range of Doppler frequency estimation, which is inversely proportional to the number of antenna elements. A simulated annealing algorithm was used for ASP optimization based on the Fisher information matrix, with the drawback that simulated annealing may converge to local minima instead of finding the global optimum [15]. For a realistic antenna array, the optimal ASP was found using a simulated annealing algorithm, and the effect of ASP on the ambiguity function was studied [16]. ASP optimization based on the objective function derived from the space-alternating generalized expectation maximization (SAGE) algorithm has been evaluated, showing that different ASPs not only extend the Doppler frequency estimation range, but also affect the side lobes of the objective function and consequently the robustness to noise [17]. To extend the study, a model of the MIMO channel sounding system based on the concept of bispatiotemporal apertures and using side-lobe level as a figure of merit to noise immunity was proposed [18].

III. ANTENNA SWITCHING PATTERN OPTIMIZATION

The impact of the CFO on the phase shifts at the antenna elements and the error in the DoA estimation are investigated using the signal model. Subsequently, the switching patterns are optimized to combat the influence of the CFO-induced phase shifts on the DoA estimation.

A. SIGNAL MODEL AND PROBLEM FORMULATION

Single-RF chain system model is studied with a M-element antenna array at the receiver and single antenna element at the transmitter considering a transmitted continuous wave (CW) signal $s_{Tx}(t)$, received signal $\mathbf{s}_{Rx}(t)$, and the CFO (Δf) effect as shown in Fig. 1. The transmitted signal is attenuated, delayed, and at the receiver down-converted with a receiver carrier frequency that is different from the transmitter carrier frequency f_c due to the CFO effect, i.e., the combined effect of carrier mismatch and a Doppler frequency shift due to the motion of the receiver or transmitter. The received signal is given by

$$\mathbf{s}_{Rx}(t) = \Re\{\, e^{\jmath 2\pi\cdot\Delta f\cdot t} e^{-\jmath\Phi}\cdot\mathbf{H}\}, \tag{1}$$

where the transmitted signal has unit amplitude, and Φ is the initial phase of the receiver's carrier signal. Here, $\mathbf{H}$ represents the channel gain vector, with each element $H_i = a_i\ e^{-\jmath 2\pi f_c \frac{d_i}{c}}$, where a_i and d_i denote the attenuation and distance between the transmitter and the i-th antenna element, respectively, for $i = 1, \ldots, M$, and c represents the speed of light.

Taking the point O as a reference, which is a distance d_0 away from the transmitter, the received signal at the antenna elements is expressed as

$$\mathbf{s}_{Rx}(t) = \Re\{a\ e^{\jmath 2\pi\Delta f t}\ e^{-\jmath\Phi}\ e^{-\jmath 2\pi f_c \frac{d_0}{c}}\mathbf{A}(\theta)\}, \tag{2}$$

where $\mathbf{A}(\theta) = [e^{-\jmath\mathbf{kr_1}}, e^{-\jmath\mathbf{kr_2}}, \ldots e^{-\jmath\mathbf{kr_M}}]^T$ is the antenna array steering vector denoting the phase shift due to DoA of the received signal at each element with respect to the antenna array reference point O, $\mathbf{r_i}$ is the vector from O to the i^{th} element, $\mathbf{k} = \mathbf{j}\frac{2\pi}{\lambda}$ is the wavenumber, λ is the wavelength of a CW signal, $\mathbf{j}$ is a unit vector in the direction of plane wave propagation, and a is the attenuation, which we assume to be the same for all antenna elements.

In single-RF chain systems, where only one antenna element samples the signal at a time, the sampling times for each antenna element must be specified. Assuming that each antenna element samples the signal once per cycle over N identical cycles and that $\mathbf{A}_{st}$ is a vector, where the value at the index i represents the i-th antenna element switch on index ranging from 1 to M, then the phase shifts due to DoA and CFO Δf at i-th antenna element are

$$\Delta\phi_i[n]\ = e^{-\jmath\mathbf{kr_i}}\ e^{\jmath 2\pi\Delta f(\mathbf{A}_{st}[i]-1+n\cdot M)T_s}, \tag{3}$$

where T_s is the sampling time and n is the index of the cycle in which the samples are taken raging from 0 to N.

The modified steering vector $\mathbf{A}'(\theta, \Delta f)$, accounting for phase shifts due to CFO Δf, which also represents the sampled phase differences on antenna elements, is then defined as

$$\mathbf{A}'(\theta, \Delta f)[n] = \begin{bmatrix} e^{-\jmath\mathbf{kr_1}}\ e^{\jmath 2\pi\Delta f(\mathbf{A}_{st}[1]-1+n\cdot M)T_s} \\ e^{-\jmath\mathbf{kr_2}}\ e^{\jmath 2\pi\Delta f(\mathbf{A}_{st}[2]-1+n\cdot M)T_s} \\ \vdots \\ e^{-\jmath\mathbf{kr_M}}\ e^{\jmath 2\pi\Delta f(\mathbf{A}_{st}[M]-1+n\cdot M)T_s} \end{bmatrix}. \tag{4}$$

For the SS ASP the $\mathbf{A}'(\theta, \Delta f)$ is

$$\mathbf{A}'(\theta, \Delta f)[n] = \begin{bmatrix} e^{-\jmath\mathbf{kr_1}}\ e^{\jmath 2\pi\Delta f\cdot(n\cdot M)\ T_s} \\ e^{-\jmath\mathbf{kr_2}}\ e^{\jmath 2\pi\Delta f\cdot(1+n\cdot M)\ T_s} \\ e^{-\jmath\mathbf{kr_3}}\ e^{\jmath 2\pi\Delta f\cdot(2+n\cdot M)\ T_s} \\ \vdots \\ e^{-\jmath\mathbf{kr_M}}\ e^{\jmath 2\pi\Delta f\cdot(M-1+n\cdot M)\ T_s} \end{bmatrix}, \tag{5}$$

Equation (4) highlights that the phase shifts at each antenna element are influenced not only by the DoA but also by the CFO, introducing errors in the DoA estimation if the CFO contribution is not addressed. The findings from paper [19] show the significant impact of neglecting CFO with SS ASP on DoA estimation with MUSIC algorithm: for example, with a sampling period of 16 μs and a CFO of 0.5 kHz, the mean absolute error across a specified DoA range exceeds 1°, demonstrating the sensitivity of DoA accuracy to even modest CFO values. The accuracy of DoA estimation is closely related to the chosen sampling period. For the validation of the proposed concepts by simulations and measurements, the sampling period of 16 μs is selected due to the hardware limitations used.

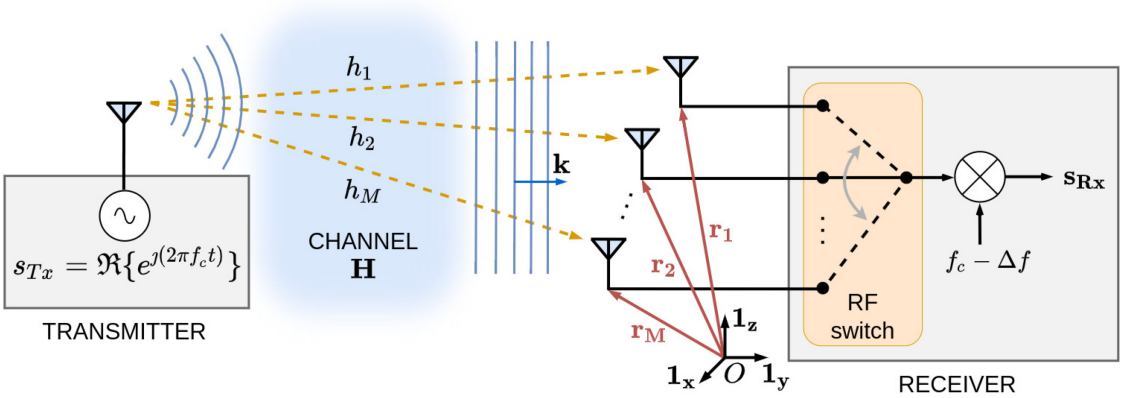

FIGURE 1. A system with a transmitter and a receiver with a single-RF chain.

B. ANTENNA SWITCHING PATTERN OPTIMIZATION METHODS

The ASP optimization techniques in this study involve two distinct approaches: spatially distributing phase progressions due to CFO associated with the antenna elements evenly around the center of the antenna array so that they contribute as noise rather than serving as a source of systematic error in DoA estimation, and using a reverse order ASP configuration to cancel out systematic error.

The evenly distributed CFO phase progressions are applied for ASP optimization in the method referred to as *EvenCFO-SP* [19]. The main design principle is to structure the ASP to result in CFO-induced phase shifts similar to additive noise, which, if sufficiently small, can be treated by the MUSIC algorithm as part of the noise subspace. The design is based on a heuristic idea in which the spatial weights are evenly distributed and counter-weighted to lower the systematic error when the CFO-induced phase shifts on the antenna elements are considered weights. The weights are spatially distributed by leveraging the order in the ASP. To find the optimal ASP based on the center of gravity calculation, an exhaustive search for the minimum cost function is performed. Optimal ASP for 8-element ULA was found to be [2, 4, 5, 6, 8, 7, 1, 3] and for 12-element UCA [2, 8, 11, 5, 6, 12, 3, 9, 10, 4, 7, 1].

The concatenation of the arbitrary order of the antenna element indices and its reverse is used in the ASP, referred to as *Mirror-SP*. The underlying principle of this method is that a particular ASP introduces a systematic error, which can be mitigated by the same ASP with the elements arranged in reverse order. This method is expected to be effective because applying an ASP in the reversed order produces error behavior equivalent to that induced by a negative CFO with the original ASP. At least two samples per antenna element are required, and the same number of samples per antenna element is needed in the reversed and the original sequence to avoid the reintroduction of systematic error. A separate or joint approach can be used to apply the reversed order ASP to the DoA estimation. In the separate approach, the DoA is first estimated separately with the arbitrary ASP in the original and reverse order. Then, the final DoA is calculated as the mean of the individual estimates. The joint approach applies the MUSIC algorithm for DoA estimation to the total samples acquired with concatenated ASPs of arbitrary ASP and its reverse order. In this study, the latter approach is considered, where the ASP is a concatenated sequence of the *SS* in original and reverse order, as shown in Figure 2, which illustrates the process of signal sampling with different ASPs during a sampling cycle, demonstrated on the example of the UCA with 12 antenna elements.

IV. EVALUATION OF DOA ESTIMATION ERRORS

We evaluated the performance improvement of DoA estimation using the MUSIC algorithm with the optimized ASPs compared to the *SS* ASP under different conditions through simulations in a MATLAB environment, focusing on two antenna array configurations: an 8-element ULA and a 12-element UCA. The DoA was estimated as the angle at which the pseudospectrum of the MUSIC algorithm reaches its maximum value. In particular, we analyzed the effects of different noise levels assuming a fixed CFO on the DoA estimation error across a range of DoA angles and investigated how different CFO values affect the DoA estimation error for a fixed DoA angle without noise. For *EvenCFO-SP*, we chose the ASPs listed in Section III-B.

A. NOISE IMPACT ON DOA ESTIMATION ERROR

The impact of different noise levels on *EvenCFO-SP* and *Mirror-SP* compared to *SS* ASP is analyzed.

The signal was generated for different DoAs over a range of signal-to-noise ratios (SNRs), with a fixed CFO of 1 kHz. DoA was estimated using the MUSIC algorithm with an angular resolution of 0.01° to calculate the pseudospectrum. To reduce the bias error due to the specific random sequence and to obtain statistically reliable results, a noise signal was generated 200 times for each SNR and the root mean squared error (RMSE) of the DoA estimates was calculated. For a ULA, the DoA ranged from 30° to 150°, where 90° corresponds to the direction perpendicular to the array axis, and for UCA it ranged from −180° to 180°. In both cases,

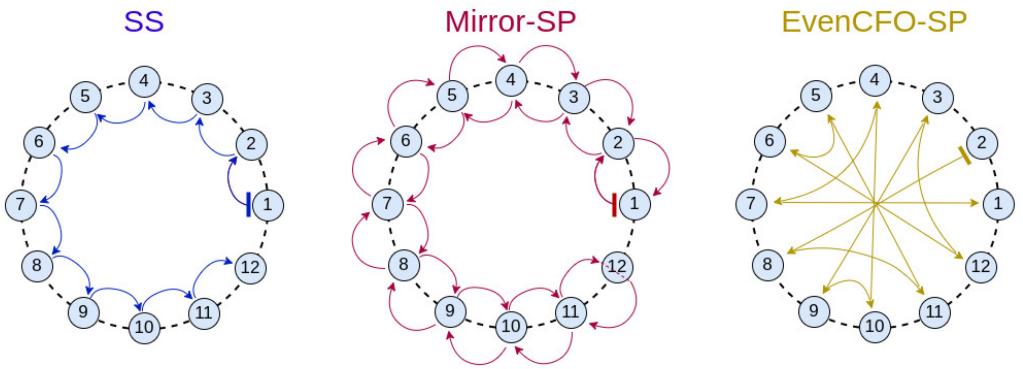

ASP method	ASP
SS	1, 2, 3, 4, 5, 6, 7, 8, 9, 10, 11, 12
Mirror-SP	1, 2, 3, 4, 5, 6, 7, 8, 9, 10, 11, 12, 12, 11, 10, 9, 8, 7, 6, 5, 4, 3, 2, 1
EvenCFO-SP	2, 8, 11, 5, 6, 12, 3, 9, 10, 4, 7, 1

FIGURE 2. Visualization of ASP methods for UCA with 12 elements.

the DoA step was 2°, the ASP was repeated sufficient times to acquire 6 IQ samples per antenna element, the carrier frequency was set to 2405 MHz, and the sampling period was 16 μs.

1) ULA EVALUATION

The RMSEs for the considered DoA range for ULA configuration and different SNRs is shown in Fig. 3. The case with 30 dB SNR serves as a reference where the noise minimises the DoA estimation error. For SNRs above 0 dB, the minimal RMSE occurs at the DoA of 90° and it increases when deviating from it, which is consistent with the ULA theory stating that the errors increase towards the end-fire directions of array [20]. As expected, the RMSEs increase with decreasing SNR. For SNRs above 0 dB, noticeably better performance is seen for *Mirror-SP* and *EvenCFO-SP* in comparison to *SS*. As the SNR decreases, the performance gain difference between the optimized ASPs and *SS* ASP is smaller, as can be seen in Table 1, showing the mean RMSE across the whole DoA range for all ASPs.

The performance gains of *Mirror-SP* and *EvenCFO-SP* compared to *SS* at an SNR of 30 dB are 2.282° and 2.287°, respectively. This decreases to 1.122° and 1.254°, respectively, for SNR of 1 dB. The SNR of 0 dB is a threshold at which noise starts to dominate over the phase shifts caused by CFO and DoA for all ASPs, and the noise effect becomes even more evident below 0 dB, leading to high RMSEs, which can be observed as a steep increase in RMSE values that are more prominent towards the end-fire directions of the array, where the system is more affected by noise. For SNRs of 1 dB and above, the *EvenCFO-SP* slightly outperforms the *Mirror-SP*, but the differences are small. Only for SNRs of 1 dB and 2 dB is the difference greater than 0.1°. This difference increases with decreasing SNR, and at high SNRs there is no significant difference.

TABLE 1. Mean RMSE of DoA estimates for 8-element ULA across the DoA range from 30° to 150° for different SNRs.

SNR	*SS*	*Mirror-SP*	*EvenCFO-SP*
30 dB	2.334°	0.052°	0.047°
20 dB	2.341°	0.165°	0.149°
10 dB	2.388°	0.524°	0.476°
6 dB	2.466°	0.845°	0.774°
3 dB	2.607°	1.247°	1.153°
2 dB	2.691°	1.441°	1.336°
1 dB	2.820°	1.698°	1.566°
0 dB	5.375°	6.945°	7.124°

2) UCA EVALUATION

RMSEs for the different DoAs, SNRs, and selected ASPs using 12-element UCA are shown in Fig. 4, and the results are summarized in Table 2.

For high SNRs, when the DoA estimation is negligibly affected by noise, the RMSE curve of the *SS* ASP has two minima approaching zero, which can be demonstrated with the results for SNR equal to 30 dB where the minima approach zero for DoAs around -105° and 75°. The RMSE curve peaks at approximately 3.66° between the minima. Fundamentally, DoA estimation algorithms compare the observed phase shifts on antenna elements with those of a set of candidate angles and look for the best match. For example, in the context of maximum likelihood estimation (MLE), one can write:

$$\hat{\theta} = \arg\min_{\phi} \sum_{i=1}^{M} \left| A_i'(\theta, \Delta f) \; - A_i(\phi) \right|^2, \tag{6}$$

where $A_i'(\theta, \Delta f)$ is the observed phase shift at the i-th antenna element, incorporating both DoA and CFO contributions, and $A_i(\phi)$ is the phase shift of a candidate

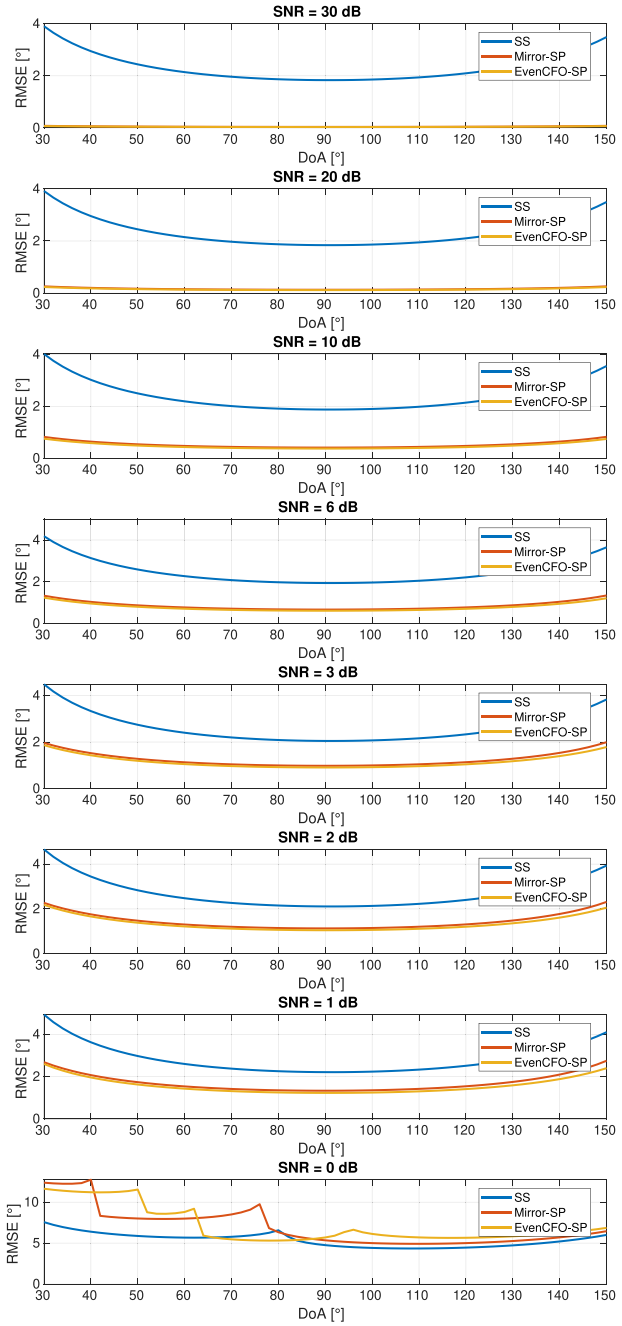

FIGURE 3. RMSE of DoA estimates for various DoAs, SNRs, and selected ASPs for the 8-element ULA, given a CFO of 1 kHz.

angle ϕ. The CFO distorts the ideal phase shifts determined by the DoA, which can make the observed phase shifts more similar to the phase shifts of an angle other than the true DoA. For UCA with a spacing of $\lambda/2$ between the antenna elements, the phase shifts due to DoA at the antenna elements are:

$$A_i(\theta) = \exp\left(-j\frac{2\pi R}{\lambda}\cos\left(\theta - \frac{2\pi\,(i-1)}{M}\right)\right), \tag{7}$$

where R is the radius of the array, and $i \in 1, , M$ is the antenna element index. The extent to which, for a given antenna element, the phase shift of neighboring angles of

TABLE 2. Mean RMSE of DoA estimates for 12-element UCA across the DoA range from -180° to 180° for different SNRs.

SNR	*SS*	*Mirror-SP*	*EvenCFO-SP*
30 dB	2.354°	0.056°	0.056°
20 dB	2.353°	0.177°	0.177°
10 dB	2.396°	0.566°	0.566°
6 dB	2.480°	0.910°	0.910°
3 dB	2.622°	1.319°	1.316°
2 dB	2.699°	1.503°	1.497°
1 dB	2.800°	1.726°	2.010°
0 dB	3.835°	3.068°	2.912°
-1 dB	10.405°	13.723°	10.007°

the true DoA is more similar to the observed phase shift compared to the ideal phase shift of the true DoA depends on the position of the cosine function at which the antenna element operates (which is determined by the true DoA) and on the magnitude of the additional CFO phase shift (which is determined by the ASP). This results in individual antenna elements favoring neighboring angles over the true DoA to varying degrees, and the overall estimation error depends on how all antenna elements collectively exhibit these preferences. For high SNRs, the minima in Fig. 4 of *SS* ASP occur when the phase shifts due to DoA and CFO best match the ideal phase shifts of true DoA, while maxima arise when the measured phase shifts best match the phase shifts of an angle farthest from the true DoA. By exploiting how the antenna elements sample the signal with different ASP configurations, we can control the amount of CFO-induced phase shifts at each antenna element to better match the ideal phase shifts of the true DoA. For example, by selecting *EvenCFO-SP*, the estimation error is zero for all DoAs as can be seen in Fig. 4 for 30 dB SNR and which is also the case for *Mirror-SP*. This shows the advantage of using optimized ASPs for accurate DoA estimation, especially for DoAs between the minima of the *SS* ASP curve.

The *Mirror-SP* and *EvenCFO-SP* show a comparable performance down to an SNR of 1 dB, achieving similar mean RMSE values. In contrast, *EvenCFO-SP* shows slightly better performance in the case of the ULA. At an SNR of 1 dB, the *EvenCFO-SP* already exhibits some significant rectangle-shaped peak errors, whereas this is not the case for the other two ASPs. This indicates a low SNR threshold for *EvenCFO-SP* and that the estimation for some DoAs is more susceptible to noise. At an SNR of 0 dB, all ASPs exhibit multiple rectangle-shaped peak errors for DoAs more susceptible to noise, indicating that the influence of noise is significant for all ASPs, and at -1 dB the errors appear more random due to even higher noise level. Compared to *SS*, the *Mirror-SP* and *EvenCFO-SP* exhibit 1.196° to 1.830° lower mean RMSE for SNRs of 2 dB to 10 dB and above 2° for higher SNRs, as can be seen in Table 2.

B. CFO IMPACT ON DOA ESTIMATION ERROR

The noise impact on DoA estimation at a fixed value of CFO is analyzed in Section IV-A, while in this subsection,

we analyze the impact of different values of CFO on DoA estimation accuracy. We limit our analysis to DoAs of 90° and 60° for the ULA test case and −10°, 30° and 75° for UCA. In this respect, the analysis was carried out in the CFO range between −50 kHz and +50 kHz without adding Gaussian noise to the signal. The DoA was estimated using the MUSIC algorithm, and the absolute error (AE) was calculated for each CFO value.

1) ULA EVALUATION

The AEs for the different CFOs, ASPs, and DoAs when ULA is used, are shown in Fig. 5. The blue curve shows the AEs for the *SS* ASP. By comparing the *SS* curves for DoAs of 90° and 60°, it is evident that the curve for 90° is symmetric around the zero CFO line, while the symmetry does not exist for 60°. This can be explained by considering the scenario with two antenna elements, where the DoA denoted as θ is estimated based on the phase shift denoted as $\Delta\Phi$ between the antenna elements, according to the relationship

$$\theta = \arccos\left(\frac{\Delta\Phi\,\lambda}{2\pi\,d}\right), \tag{8}$$

where d is the distance between antenna elements. $\Delta\Phi$ is the sum of $\Delta\Phi_{DoA}$, which is the phase shift due to the different travel distances depending on DoA, and the $\Delta\Phi_{CFO} = 2\pi\,\Delta f\,T_s$, which is the phase shift due to CFO Δf. This sum indicates that the $\Delta\Phi_{DoA}$ component establishes the operating point of the arccos function, which can then be shifted to the left or right depending on the sign of the $\Delta\Phi_{CFO}$ component, as illustrated in Fig. 6 when d is $\lambda/2$. For a DoA of 90°, $\Delta\Phi_{DoA}$ is zero, resulting in an operating point at $(0, 90°)$. The function arccos is approximately linear and symmetric when its argument is close to zero, so the value of the function for a positive CFO is equal to its negative counterpart. This explains the symmetry and approximately linear behavior of the AE curve of *SS* for low CFO values.

However, the arccos function exhibits non-linearity for non-zero arguments, resulting in different AEs for DoAs that deviate from 90° when a positive CFO is compared to its negative counterpart. The further the DoA deviates from 90°, the greater the asymmetry and slope of the curve, resulting in larger AEs caused by the CFO.

Comparison of AE curves for *SS* for DoAs of 60° and 90° in Fig. 5 shows a steeper slope near 0 Hz CFO for DoA of 60°, leading to larger AEs. The CFO frequency at which the AE of the *SS* ASP reaches its maximum is determined when the argument of the arccos function is 1. If d is $\lambda/2$, this frequency is calculated as $\Delta f = \frac{\pm 1 - \cos(\theta)}{2T_s}$. It is also worth noting that the ASP with the reversed elements of the *SS* sequence produces a curve that mirrors the *SS* ASP curve around zero CFO line.

Mirror-SP and *EvenCFO-SP* are represented by the red and yellow curves, respectively. For small absolute values of CFO, the AEs for both ASPs and both considered DoAs are 0°, demonstrating the proposed CFO-independent DoA estimation approach, which is the aim of this paper.

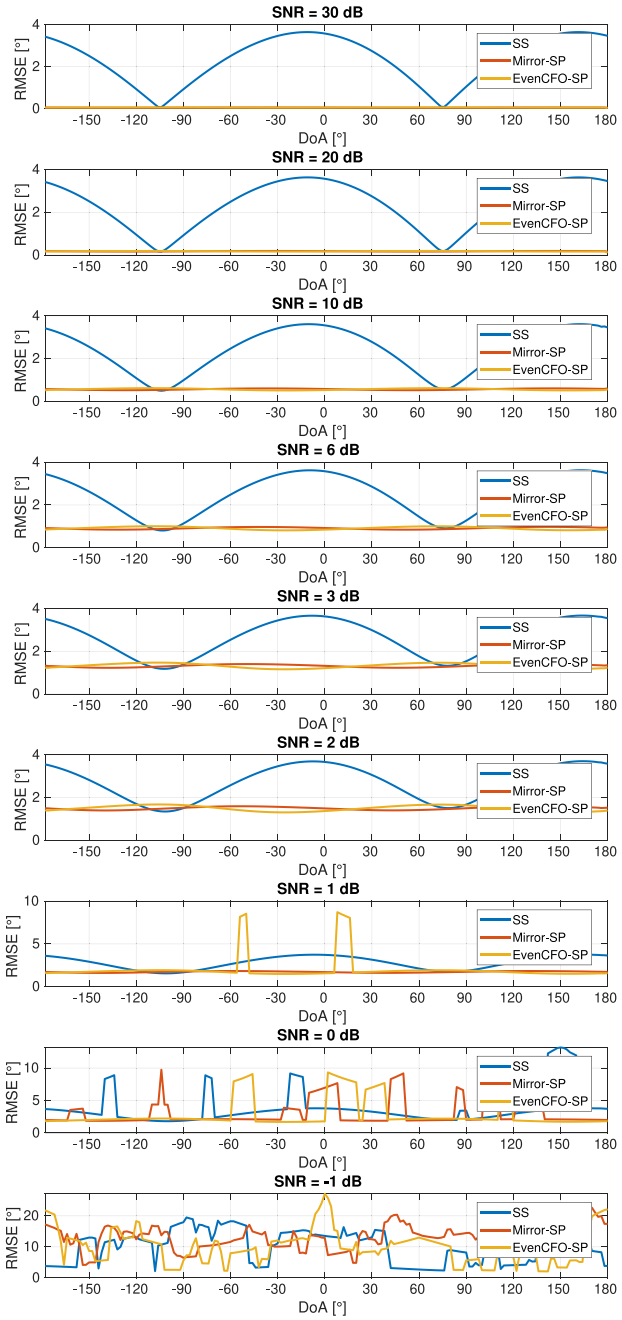

FIGURE 4. RMSE of DoA estimates for various DoAs, SNRs, and selected ASPs for a UCA with 12 elements, given a CFO of 1 kHz.

At ±3900 Hz, the AE of *Mirror-SP* jumps instantaneously, indicating the low and high frequency bounds of the CFO, beyond which the proposed approach is no longer effective. Empirical analysis based on our observations have shown that these bounds are independent of DoA, the configuration of the antenna elements and the number of samples per antenna element, and for the MUSIC algorithm are equal to $\pm 1/(2\,T_s\,M)$. Beyond these bounds, an ambiguity between two peaks in the MUSIC pseudospectrum is observed, leading to DoA estimation errors similar to those when

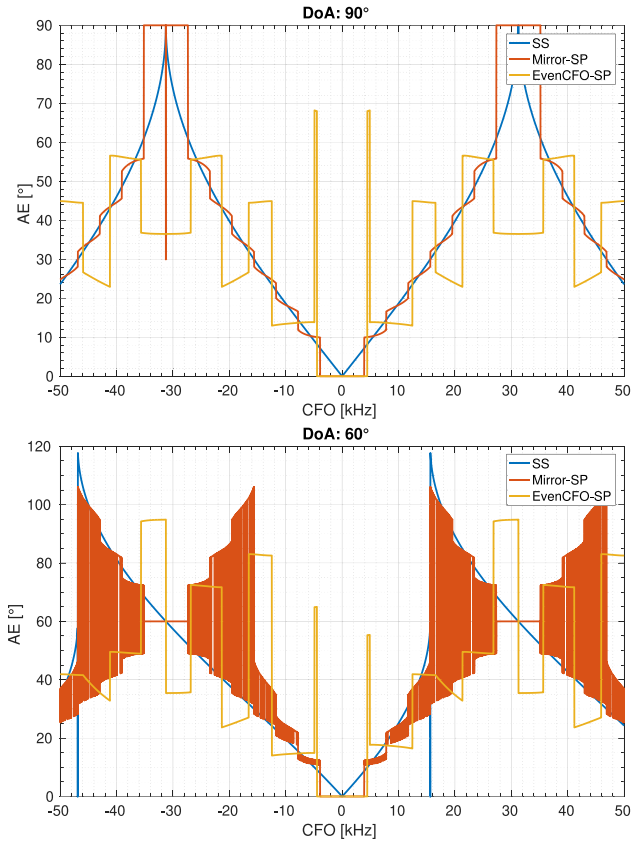

FIGURE 5. AEs of different CFOs at fixed DoA for 8-element ULA with no added noise.

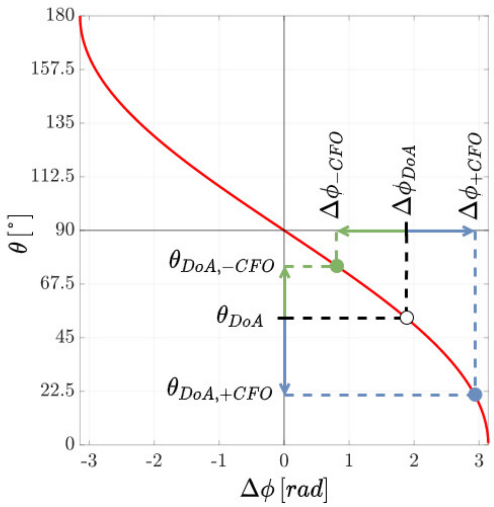

FIGURE 6. CFO effect on DoA estimation.

using *SS* ASP and ASP with reverse order elements of *SS*. This effect is shown in Fig. 7, where two MUSIC pseudospectra are depicted: one with CFO within the identified frequency bounds, demonstrating the optimal performance of *Mirror-SP*, and another with CFO exceeding these bounds, demonstrating the two-peak ambiguity problem, where none of the peaks have the position at the correct

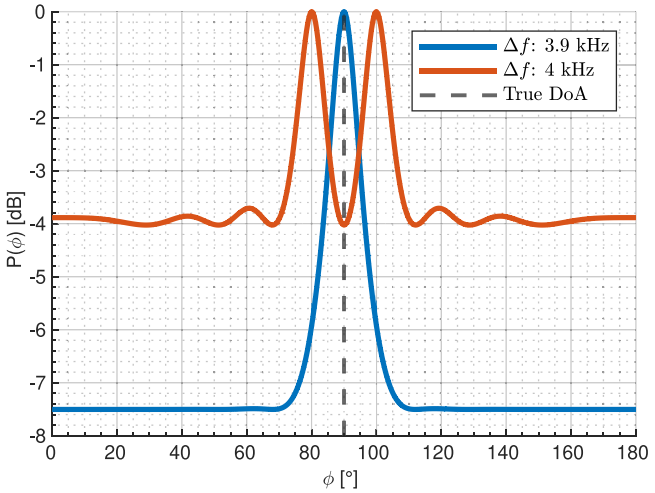

FIGURE 7. MUSIC pseudospectra for ULA and the DoA of 90° showing the impact of CFO on the pseudospectrum when *Mirror-SP* is used for CFO below (3.9 kHz) and above (4 kHz) the frequency bound.

angle. If the *SS* ASP or its reverse order counterpart are individually employed for DoA estimation under CFO conditions, both produce a single dominant peak in the MUSIC pseudospectrum: the *SS* ASP yields a peak that is shifted relative to the true DoA due to the CFO, while its reverse order counterpart yields a peak that is shifted equivalently to the scenario of using *SS* ASP with a negative CFO. Since *Mirror-SP* is a concatenation of these two ASPs, the resulting pseudospectrum of *Mirror-SP* also contains two peaks at approximately the same positions as those of the individual ASPs, although not exactly the same due to the mutual influence of the peaks. Due to numerical errors inherent in the computational process, there are small differences in amplitude between these peaks. Since the DoA is determined by finding the angle corresponding to the highest peak, these small numerical fluctuations lead to frequent instantaneous jumps in AE beyond the CFO frequency bounds, whose envelopes approximately follow the AE curves of the *SS* ASP and its mirrored version around the zero CFO line corresponding to *SS* ASP with reversed order of the elements. Within the CFO bounds, *Mirror-SP* performs optimally because the two peaks in the MUSIC pseudospectrum remain closely spaced and due to the limited resolution of the MUSIC algorithm, they are effectively merged into a single peak centered at their mean position, which coincides with the correct DoA.

Similar to *Mirror-SP*, the CFO bounds for *EvenCFO-SP* are observed at ± 4450 Hz, which are slightly higher than those of *Mirror-SP* and are also independent of DoA, antenna elements configuration, and the number of samples per antenna element. Beyond these bounds, the errors are high but change less frequently than for *Mirror-SP*. The effect of different CFOs manifest as distinct patterns of peaks in the MUSIC pseudospectrum. When the CFO is close to zero, a single dominant peak corresponding to the correct DoA estimate is observed. As the CFO increases, a

secondary peak emerges that increases in size. As long as this secondary peak is lower than the primary peak, the correct DoA estimate is maintained. However, if the CFO continues to increase, the secondary peak exceeds the primary peak in magnitude and becomes the dominant peak. This transition leads to a sudden jump in the estimation error, marking the CFO bounds. As the CFO continues to increase, yet another peak appears, repeating the pattern of a new peak gradually strengthening until it dominates the pseudospectrum causing a sudden jump in the estimation error. This behavior explains the observed jumps in the AE curve, with relatively stable regions in between.

Although it may initially seem advantageous to use *SS* ASP, given that *EvenCFO-SP* has limited CFO bounds where the AE increases significantly, the AEs of *SS* ASP at CFO bounds of *EvenCFO-SP* are already 8.23° for a DoA of 90° and are even larger for DoAs that deviate from 90°. For a DoA of 60° the errors are 10.03° and 9.1°. These errors are insufficient for most applications. The significant jump in error can also be seen as an advantage when estimating DoA from several consecutive estimates, as outliers can be easily detected.

It is worth noting that CFO bounds of optimized ASPs may vary with the choice of DoA search algorithm. We observed differences when using MUSIC, MLE and angle-FFT, as the algorithms may react differently to CFO-induced phase distortions. The CFO bounds presented here are specific to the MUSIC algorithm and may change for other algorithms. Although a detailed analysis is beyond the scope of this paper, this remains an interesting direction for future research.

The AE of *SS* ASP, and consequently the performance improvement of the proposed methods within CFO bounds, can be calculated using (8) as follows:

$$AE = |\arccos(cos\theta + 2 \cdot \Delta f \cdot Ts) - \theta|. \tag{9}$$

In linear region of arccos and for angles close to 90° the relation approximates to

$$AE \approx 2 \cdot |\Delta f| \cdot Ts. \tag{10}$$

2) UCA EVALUATION

For the UCA analysis, we chose DoAs of −10°, 30°, and 75° to capture a range of AE behaviors associated with the *SS* ASP, which is DoA dependent and has two minima with a peak in between, as shown in Fig. 4. For a DoA of -10° (which roughly corresponds to the maximum of *SS* ASP in Fig. 4), the optimized ASPs should provide the largest performance gain, while no gain is expected at 75° (which corresponds to the minimum of *SS* ASP in Fig. 4). The DoA of 30° represents a medium-case scenario with moderate improvement potential. Fig. 8 shows the AEs for different CFOs for the aforementioned DoAs.

The results for DoAs of −10° and 30° show that for small absolute CFO values (close to 0 Hz) the AEs of the *SS* ASP increase approximately linearly, whereby the AEs for a DoA of −10° are larger than those for 30°, which is consistent with the positions of the maxima from the results in Fig. 4. In contrast, both *Mirror-SP* and *EvenCFO-SP* have zero AEs, demonstrating their effectiveness in eliminating the CFO effect in DoA estimation within their CFO bounds. At higher absolute values of CFO, all three ASPs show significant jumps in DoA estimation errors. For *Mirror-SP*, the CFO frequency bounds occur at ±2600 Hz, which is lower than in the ULA case due to the larger number of antenna elements used. In contrast, the CFO bounds for *EvenCFO-SP* are slightly higher than those for *Mirror-SP* and are DoA dependent, with not necessarily equal positive and negative bound. Across all angles, none of the ASPs exhibit symmetry about the zero CFO line.

For a DoA of 75°, all three ASPs have 0° AEs within their CFO bounds, with the absolute bounds of *SS* ASP being the highest and those of *Mirror-SP* the lowest. Notably, the error-free estimates within the CFO bounds of *SS* ASP for this DoA coincide with the positions of the minima in Fig. 4.

For *EvenCFO-SP*, the effect of CFO on the MUSIC pseudospectrum within and beyond the CFO bounds approximately follows the patterns observed in the ULA case. For *Mirror-SP*, the behavior in UCA differs from ULA, especially beyond the CFO bounds, where the AE curve does not show frequent jumps as observed in the ULA case due to the two-peak ambiguity. Although two dominant peaks are still seen in the MUSIC pseudospectrum beyond the CFO bounds, they have unequal magnitudes, resulting in more stable AE regions where the AE curve does not change much with respect to CFO changes. At sufficiently high CFO values, the MUSIC pseudospectrum no longer resembles the two-peak structure anymore, but rather the pseudospectra of *EvenCFO-SP*. Similarly, *SS* ASP shows sharp transitions in AE curve, as the phase shifts due to DoA and CFO are not correlated in contrast to the ULA case.

V. EXPERIMENTAL VALIDATION

The experimental validation involves a comparison of *SS*, *EvenCFO-SP* and *Mirror-SP* using an 8-element ULA and a 12-element UCA [21]. For a fixed angle, different CFOs were systematically introduced at the receiver (RX), and the AEs of the DoA estimates were analyzed to compare the performance of the selected ASPs and identify the frequency bounds. The results are presented both without and with CFO calibration.

A. MEASUREMENT SETUP

Measurements were performed outdoors in a small park without close obstacles to minimize the multipath effect, which is not the focus of this paper. The transmitter (TX) was positioned at a fixed location with a transmit power of approximately 14 dBm at the output of the transceiver, and the RX was placed on a rotating stand, allowing it to rotate around the center of the antenna array. This setup enabled the estimation of DoA at multiple angles relative to the TX. For the ULA configuration, the measurement was performed

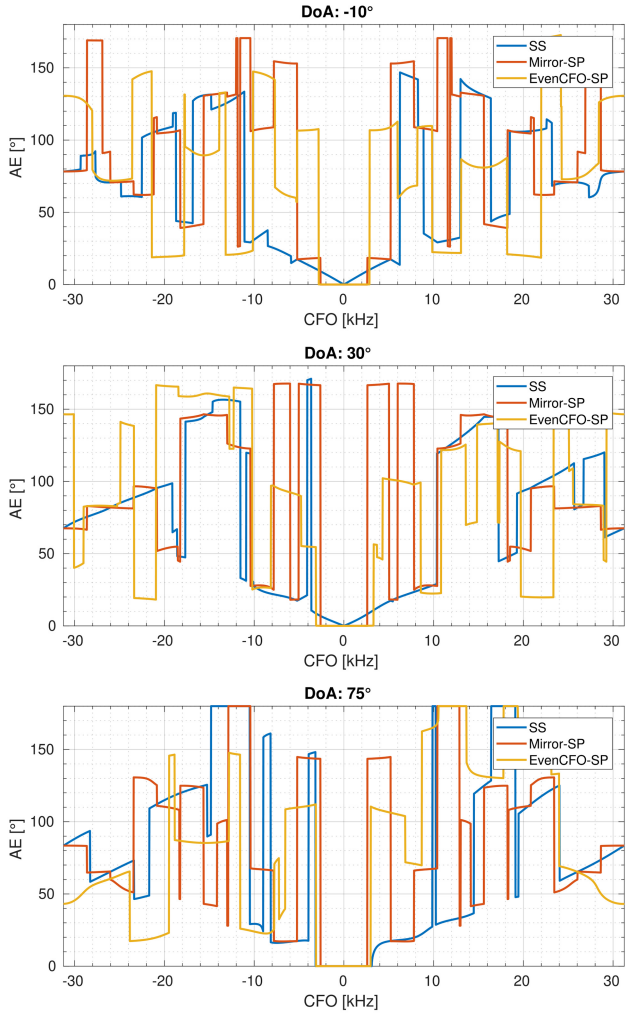

FIGURE 8. AEs of different CFOs at fixed DoA for 12-element UCA with no added noise.

at a DoA of 90°, while for the UCA the measurements were performed at −30°, 30°, and 90°. The angles for the UCA were chosen as multiples of 30° to facilitate the measurement procedure, particularly the exact positioning of the RX, and to approximately match the simulation setup.

The TX and RX were positioned 2.5 m apart to satisfy the far-field condition of the antenna arrays and mounted at the same height, approximately 1.5 m above the ground. Both antenna arrays have an antenna element spacing of 6 cm. The operating frequency was set to 2405 MHz. The initial results indicated that the activity of the nearby WiFi access points is lowest in this frequency band, resulting in reduced interference. For measurements with ULA, we used transceivers with low-cost microcontrollers [22] and an IEEE 802.15.4-compliant radio AT86RF215 with a Phase Measurement Unit (PMU) for register-based phase monitoring of the received signal [23]. We used OpenMote-B boards based on the same radio for the UCA case. To extend the single-RF signal chain of the radio, the devices incorporate a 12 or 8 channel RF switch [24]. The sampling

FIGURE 9. Measurement setup.

period was 16 μs, matching the simulation setup. The measurement setup is shown in Fig. 9.

We considered a similar implementation of the sampling and switching scheme as in [6], where the first 8 IQ samples are acquired at the reference antenna for the coarse CFO calibration, followed by sampling the signal with *SS*, *EvenCFO-SP*, and *Mirror-SP* in this order. This sampling scheme ensures that coarse calibration is performed on the same reference samples for all ASP methods, allowing for unbiased comparison unaffected by different CFO estimation results. The problem arises if CFO has a high drift. Then the CFO estimate may only be accurate for the *SS* ASP, as it follows the reference samples and may be obsolete for the other two ASPs. We assumed the CFO drift is small enough to mitigate this issue. For DoA estimation, we acquired 10 IQ samples on each antenna element in the case of ULA and 6 IQ samples in the case of UCA, which is the maximum possible considering the limitation of 90 sample slots available and maintain an even number of samples, as *Mirror-SP* performs best with even sample counts.

The measurements were performed with the RX operating at a frequency offset from the center frequency ranging from -20.196 kHz to 20.196 kHz in steps of 396 Hz, which is the minimum carrier frequency step supported by the radio. Based on prior measurements, we assumed that the CFO of the devices would be within this range. At each RX frequency offset, 50 DoA estimates were obtained using the MUSIC algorithm for the ULA case and 100 for the UCA case. Since the measurements for UCA had a lower SNR, we doubled the number of DoA estimates. The AE was then calculated as the median of these 50/100 measurements minus the true angle.

Since the expected differences in performance between the selected ASPs are on the scale of several degrees, even small inaccuracies in angular positioning during the measurements could lead to significant deviations that would strongly influence the interpretation of the results. Therefore,

the measurements were first processed by applying the MLE algorithm to calculate the exact DoA and CFO for each angle set when the frequency offset at the RX was set to 0 Hz, using all collected IQ samples for a given ASP. However, these estimates showed slight variations between ASPs due to additional factors such as hardware imperfections, CFO drift, etc. To address this differences, the average of the estimated DoAs of all ASPs was taken as the calibrated angle, which was subsequently used as the true reference angle for the measurement setup.

B. ULA EXPERIMENTAL EVALUATION

The AE as a function of the frequency offset at the RX for the ULA case without CFO calibration is shown in Fig. 10(a). The *SS* ASP is used as a reference, as it is expected that the AE reaches its minimum at the frequency offset that compensates for the real CFO of the devices due to hardware imperfections. For our TX-RX pair, this occurs at a value slightly above 5 kHz, and is referred to as the compensated CFO point (CCFOP). For this reason, the curves in Fig. 10(a) are shifted for the real CFO value compared to the simulation results in Fig. 5. The results demonstrate a linear trend in AE growth as the frequency offset deviates from the CCFOP, aligning with the simulation findings presented in Section IV-B. There is also a good alignment between simulation and measurement results for the optimized ASPs.

We empirically define a flat region as a region within the positions of a rapid jump in the AE that resembles a step-like transition corresponding to CFO bounds. For *EvenCFO-SP* the mean and standard deviation of AEs within the flat region are 0.14° and 0.07°, respectively, while for *Mirror-SP* they are 0.47° and 0.28°. The slightly higher AEs observed for *Mirror-SP* can be attributed to its greater sensitivity to noise, as shown with simulations in Section IV-A, as well as to the imperfect process of true angle calibration. For comparison, the mean and standard deviation of the AEs for the *SS* ASP within the flat region of *EvenCFO-SP* are 4.32° and 2.60°, while within the flat region of *Mirror-SP* they are 3.81° and 2.15°, respectively.

The flat region of *EvenCFO-SP* has a width of $BW_{CFO} =$ 8.316 kHz, while the width of *Mirror-SP* is $BW_{CFO} =$ 7.524 kHz, which agrees with the simulation results where the *EvenCFO-SP* region is 2×4450 Hz$=$ 8900 Hz wide and the *Mirror-SP* region is 2×3900 Hz$=$ 7800 Hz wide, especially considering that the minimum frequency step is 396 Hz and that additional simulations with noise have shown that BW_{CFO} decreases as the noise level increases. The measured results show a difference between the center frequencies of the flat regions for *EvenCFO-SP* and *Mirror-SP*, which should be the same according to the simulation results in Section IV-B. This deviation indicates a drift in actual CFO between the measurements for *EvenCFO-SP* and *Mirror-SP*.

A disadvantage of *EvenCFO-SP* is that significant errors can occur if the CFO values are outside the flat region. In

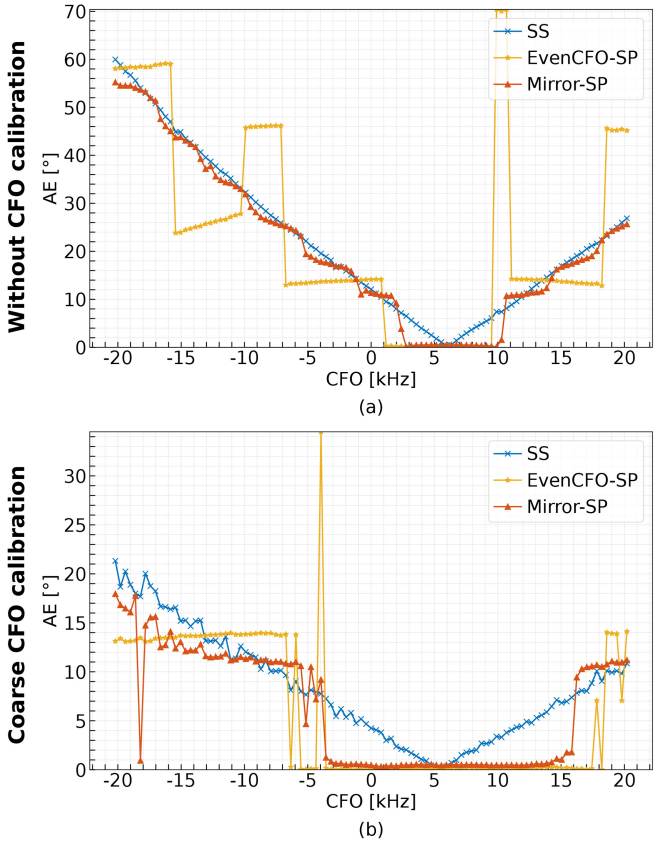

FIGURE 10. AEs for ULA for DoA of 90° considering different frequencies offset at RX without and with coarse CFO calibration.

contrast, *Mirror-SP* shows error behavior similar to that of *SS* ASP in such cases. To ensure optimal performance of optimized ASPs, it is crucial that the CFO is within the frequency bounds ($|\Delta f| < BW_{CFO}/2$). Since these bounds may be too low for some IoT devices, optimized ASPs combined with a coarse CFO estimation and calibration offer a computationally efficient alternative. This approach only requires sufficient accuracy of the CFO calibration to ensure that the corrected CFO remains within the frequency bounds of the specific ASP. To implement this approach, coarse CFO estimation and calibration was performed on 8 reference samples sampled with antenna 1, which was chosen arbitrarily. Since the signal is sampled at 1/8 of the baseband frequency, the CFO remains the only frequency component in the sampled signal. The CFO was estimated using a Fourier transform with a zero padding of length 256, followed by a parabolic interpolation considering the first neighborhood samples as described in [6]. DoA estimation was then performed on the corrected phase samples as described above. The results are shown in Fig. 10(b). If the CFO calibration were perfect, all ASPs would have an error of 0° across all Rx frequency offsets. However, due to the limited number of samples available, limited CFO estimation resolution, hardware imperfections such as sampling time inaccuracies and the relatively short observation period used for the CFO estimation, errors are to be expected.

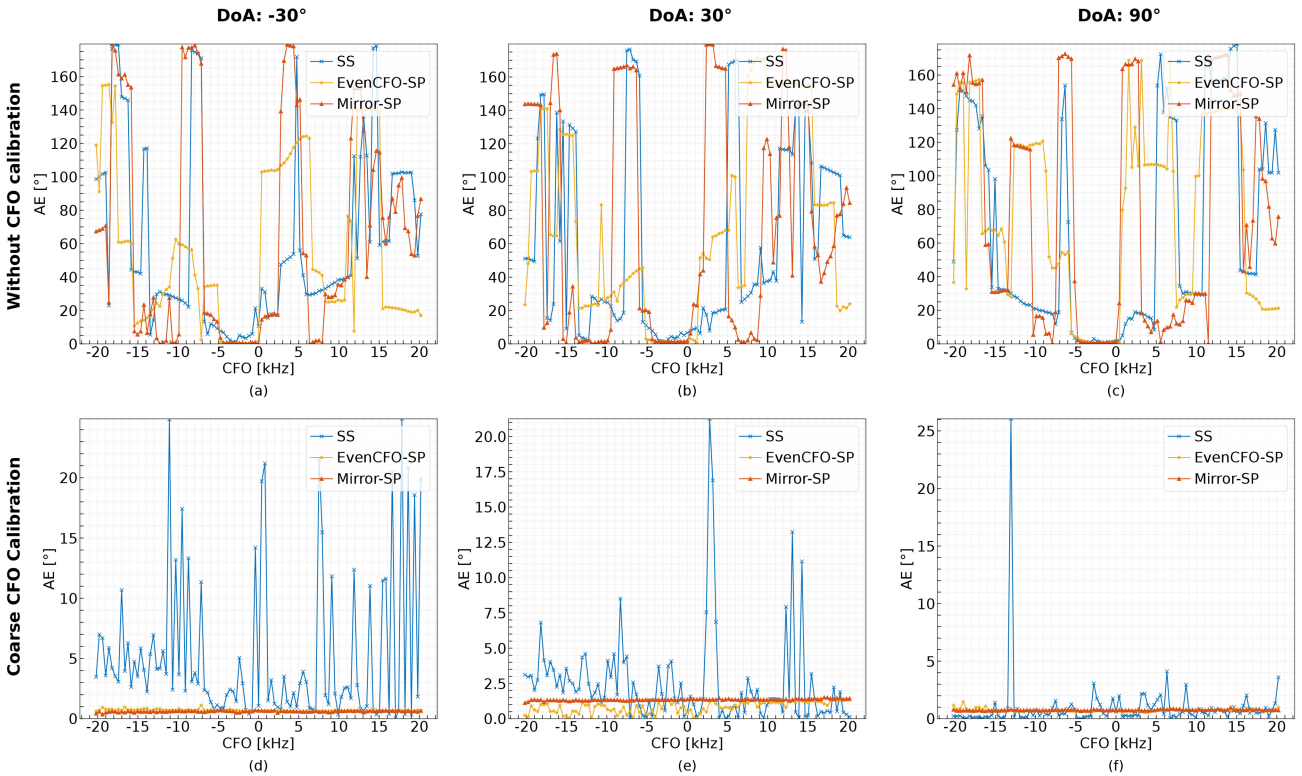

FIGURE 11. AEs for UCA for DoAs of -30°, 30°, and 90° considering different frequencies offset at RX without and with coarse CFO calibration.

The results show that with coarse CFO calibration, the flat regions around the CCFOP point of *EvenCFO-SP* and *Mirror-SP* are larger than in the case without CFO calibration, indicating that the CFO calibration was partially successful. For regions outside the flat regions of *EvenCFO-SP* and *Mirror-SP*, similar conclusions can be drawn as from the results without CFO calibration. With more accurate CFO estimation, the wider flat regions of *EvenCFO-SP* and *Mirror-SP* are expected. The mean value and standard deviation of AEs of *EvenCFO-SP* within its flat region are 0.10° and 0.07°, respectively, while for *Mirror-SP*, they are 0.60° and 0.30°. For comparison, the calculated mean and standard deviation of the AEs for the *SS* ASP within the flat region of *EvenCFO-SP* are 4.01° and 2.36° and within the flat region of *Mirror-SP* they are 3.68° and 2.12°.

TABLE 3. Comparison of ASPs in DoA estimation metrics for UCA without CFO calibration.

ASP	Metric	-30°	30°	90°
EvenCFO-SP	Mean	0.79°	1.35°	1.59°
	Std	0.32°	0.64°	1.57°
	BW_{CFO}	4752 Hz	6336 Hz	5940 Hz
SS*	Mean	6.07°	5.58°	1.71°
	Std	5.09°	3.10°	1.58°
Mirror-SP	Mean	0.51°	1.59°	1.03°
	Std	0.27°	0.44°	0.37°
	BW_{CFO}	4356 Hz	4356 Hz	4752 Hz
SS**	Mean	5.94°	4.20°	1.19°
	Std	5.28°	2.22°	0.78°

* SS within the *EvenCFO-SP* flat region
** SS within the *Mirror-SP* flat region

C. UCA EXPERIMENTAL EVALUATION

AEs for UCA at different RX frequency offsets without CFO calibration are shown in Fig. 11(a)-(c). Due to the use of different transceiver devices for the UCA measurements, the CCFOP differs from the ULA case and is approximately -2.3 kHz. Although the measurements with UCA have higher noise compared to the ULA measurements, the flat regions where *EvenCFO-SP* and *Mirror-SP* perform optimally are clearly visible.

Mean values and standard deviations (Std) of AEs within the flat regions of the optimized ASPs are listed in Table 3. These values are compared with those of the *SS* whose samples are within the same flat regions of the corresponding optimized ASP. As predicted by the simulations, the performance gain of the optimized ASPs compared to *SS* is highest at a DoA of -30°, with the difference in mean value between *SS* and *EvenCFO-SP* being 5.28° and the difference between *SS* and *Mirror-SP* being 5.43°. The performance gain is lower for a DoA of 30°, with differences in mean value of 4.23° for *SS* versus *EvenCFO-SP* and 2.61° for *SS* versus *Mirror-SP*. The smallest performance gain occurs at a DoA of 90°, where the mean values for *SS*, *EvenCFO-SP* and *Mirror-SP* are almost identical. Due to the high noise

TABLE 4. Comparison of ASPs in DoA estimation metrics for UCA with coarse CFO calibration.

ASP	Metric	-30°	30°	90°
EvenCFO-SP	Mean	0.70°	0.84°	0.75°
	Std	0.08°	0.39°	0.12°
Mirror-SP	Mean	0.61°	1.35°	0.76°
	Std	0.05°	0.06°	0.05°
SS	Mean	5.31°	2.50°	0.96°
	Std	6.22°	3.27°	2.60°

level, a direct comparison between *EvenCFO-SP* and *Mirror-SP* is difficult; however, the measurements indicate similar performance for both. The measured BW_{CFO} are slightly lower than the simulated values, which is also observed for the ULA case. The higher measured BW_{CFO} of *EvenCFO-SP* compared to that of *Mirror-SP*, agrees with the simulations.

AEs for UCA at different RX frequency offsets with coarse CFO calibration, as previously described for the case of ULA, are shown in Fig. 11(d)-(f). In this case, the coarse CFO calibration proved to be sufficiently accurate for all DoAs, so that the flat regions of the optimized ASP extend over the entire RX frequency offsets. The CFO estimates achieved higher accuracy compared to the ULA case due to lower sampling time inaccuracies in the hardware used for the measurements with the UCA. The AEs of the *SS* ASP are more scattered as they depend on the efficiency of the CFO calibration compared to the AEs of the optimized ASP. The standard deviations of the ASPs are listed in Table 4 showing that the scatter of the *SS* AEs is highest for DoA of -30°, lowest at 90° and in between at 30°, which is consistent with the AEs of *SS* as a function of CFO within the flat regions of the optimized ASPs, as shown in Section IV-B. For a DoA of 90°, the mean value of the AEs of *SS* is comparable to the optimized ASPs. For DoA of -30°, the difference in the mean value between *SS* and *EvenCFO-SP* is 4.61° and the difference between *SS* and *Mirror-SP* is 4.70°. For DoA of 30°, these differences are 1.66° and 1.15° for *EvenCFO-SP* and *Mirror-SP*, respectively.

VI. CONCLUSION

In this study, we addressed the challenge of minimizing the effect of CFO on DoA estimation without increasing computational complexity. Compared to the standard *SS* approach, we demonstrated the performance improvements of two optimized ASPs, *EvenCFO-SP* and *Mirror-SP*. The three ASPs were evaluated under two antenna array configurations: the ULA and UCA. Through simulations, we analyzed the impact of noise on DoA estimation accuracy for all three ASPs at various angles. The results indicate that the performance gain of the optimized ASPs decreases with decreasing SNR. Additional simulations examined how varying CFO levels influence the AE of the optimized ASPs, revealing that each has specific CFO bounds within which it performs optimally. The results of the experimental validation are consistent with the simulations, affirming that when a coarse CFO correction is applied, the CFO bounds for optimal performance can be extended. This correction can be implemented with lower computational cost, achieving accuracy within the kHz range, compared to fine CFO estimation. Consequently, optimized ASPs are well suited for embedded or IoT devices with limited computational resources. This approach also allows fewer IQ samples to be allocated to CFO estimation, increasing the number of samples available for DoA estimation, which improves localization accuracy. The advantage of the optimized ASP approaches used in this study is that they avoid the computationally impractical exhaustive ASP search required by previous methods to find the optimal ASP, as they are independent of the number of antenna elements, with *Mirror-SP* using any ASP as a basis and *EvenCFO-SP* employing a heuristic strategy. Although the focus of this paper is on the performance gain by using optimized ASP for DoA optimization with the MUSIC algorithm, we have observed a similar performance gain also for the angle-FFT algorithm and parametric algorithms such as maximum likelihood estimation (MLE), provided that the search parameter is restricted to DoA and the CFO is assumed to be zero. Furthermore, we anticipate that similar conclusions can be applied to other subspace-based DoA estimation algorithms such as Estimation of Signal Parameters via Rotational Invariant Techniques (ESPRIT) and Root-MUSIC. In future work, we plan to extend antenna switching optimization by considering different switching schemes in the sampling cycles, modify *Mirror-SP* to use different base switching schemes, and investigate how the optimized ASPs effectively mitigate the CFO effect in DoA estimation with algorithms other than MUSIC.

REFERENCES

[1] Y. Li et al., "Toward location-enabled IoT (LE-IoT): IoT positioning techniques, error sources, and error mitigation," *IEEE Internet Things J.*, vol. 8, no. 6, pp. 4035–4062, Mar. 2021. [Online]. Available: https://ieeexplore.ieee.org/document/9184896

[2] F. Zafari, A. Gkelias, and K. K. Leung, "A survey of indoor localization systems and technologies," *IEEE Commun. Surveys Tuts.*, vol. 21, no. 3, pp. 2568–2599, 3rd Quart., 2019. [Online]. Available: https://ieeexplore.ieee.org/document/8692423

[3] N. Paulino and L. M. Pessoa, "Self-localization via circular Bluetooth 5.1 antenna array receiver," *IEEE Access*, vol. 11, pp. 365–395, 2023. [Online]. Available: https://ieeexplore.ieee.org/document/10003199

[4] Y. Yuan, C. Liu, L. Zhou, Z. Xu, Z. Liu, and K. Ma, "Improving AOA accuracy in BLE-based Localization with a hierarchical estimation framework and phase correction mechanism," *IEEE Trans. Instrum. Meas.*, vol. 73, pp. 1–10, 2024. [Online]. Available: https://ieeexplore.ieee.org/document/10643481

[5] "Bluetooth core specification, V.5.1," Bluetooth, SIG, Kirkland, WA, USA, Rep. 5.1, 2019. Accessed: Nov. 18, 2024. [Online]. Available: https://www.bluetooth.com/specifications/specs/core-specification-5-1/

[6] G. Morano, A. Simončič, T. Kocevska, T. Javornik, and A. Hrovat, "Angle of arrival estimation using IEEE 802.15.4 TSCH protocol," in *Proc. IEEE 34th Annu. Int. Symp. Pers., Indoor Mobile Radio Commun. (PIMRC)*, 2023, pp. 1–7. [Online]. Available: https://ieeexplore.ieee.org/document/10293886/

[7] D. Xiao, S. Hu, K. Kang, and H. Qian, "An improved AoA estimation algorithm for BLE system in the presence of phase noise," *IEEE Trans. Consum. Electron.*, vol. 69, no. 3, pp. 400–407, Aug. 2023. [Online]. Available: https://ieeexplore.ieee.org/document/10064356

[8] S. Cloudt, "Bluetooth low energy direction finding on embedded hardware by mitigating carrier frequency offset and multipath fading," M.S. thesis, Math. Comput. Sci., Eindhoven Univ. Technol., Eindhoven, The Netherlands, 2021.

[9] L. Yao, "Bluetooth direction finding," M.S. thesis, Delft Univ. Technol., Delft, The Netherlands, 2018. [Online]. Available: https://repository.tudelft.nl/islandora/object/uuid

[10] P. Avital, G. Chardon, and J. Picheral, "Design of switching sequences for sine parameters estimation on switched antenna arrays," *Signal Process.*, vol. 188, Nov. 2021, Art. no. 108244. [Online]. Available: https://www.sciencedirect.com/science/article/pii/S0165168421002814

[11] L. Yi, T. Guo, M. Guo, and Y. Fu, "Motion compensation for SAA FMCW radar based on specific switching scheme," *Appl. Sci.*, vol. 9, p. 3441, Aug. 2019.

[12] L. Yi, K. Yang, M. Guo, and Y. Fu, "Elimination of motion-induced phase based on double-time switching scheme for SAA FMCW radar," *Electronics*, vol. 8, p. 786, Jul. 2019.

[13] P. Feil, "Optimizing switching sequence in the case of switched antenna arrays," U.S. Patent 182 174 A1, Jul. 2012. [Online]. Available: https://patents.google.com/patent/US20120182174A1/en

[14] C. Hu, Y. Liu, H. Meng, and X. Wang, "Randomized switched antenna array FMCW radar for automotive applications," *IEEE Trans. Veh. Technol.*, vol. 63, no. 8, pp. 3624–3641, Oct. 2014. [Online]. Available: https://ieeexplore.ieee.org/document/6750120

[15] A. Al-Ameri, J. Park, J. Sanchez, X. Cai, and F. Tufvesson, "A hybrid antenna switching scheme for dynamic channel sounding," in *Proc. IEEE 97th Veh. Technol. Conf. (VTC-Spring)*, Jun. 2023, pp. 1–6. [Online]. Available: https://ieeexplore.ieee.org/document/10199525

[16] R. Wang, O. Renaudin, C. U. Bas, S. Sangodoyin, and A. F. Molisch, "On channel sounding with switched arrays in fast time-varying channels," *IEEE Trans. Wireless Commun.*, vol. 18, no. 8, pp. 3843–3855, Aug. 2019. [Online]. Available: https://ieeexplore.ieee.org/document/8728188

[17] T. Pedersen et al., "Joint estimation of Doppler frequency and directions in channel sounding using switched Tx and Rx arrays," in *Proc. IEEE Global Telecommun. Conf.*, vol. 4, Nov. 2004, pp. 2354–2360. [Online]. Available: https://ieeexplore.ieee.org/document/1378429/authors#authors

[18] T. Pedersen, C. Pedersen, X. Yin, and B. H. Fleury, "Optimization of spatiotemporal apertures in channel sounding," *IEEE Trans. Signal Process.*, vol. 56, no. 10, pp. 4810–4824, Oct. 2008. [Online]. Available: https://ieeexplore.ieee.org/abstract/document/4579719

[19] A. Simončič, G. Morano, A. Švigelj, A. Hrovat, and T. Javornik, "Optimizing switching pattern to reduce CFO effects in single RF chain direction finding systems," in *Proc. 7th Int. Balkan Conf. Commun. Netw. (BalkanCom)*, Jun. 2024, pp. 113–118. [Online]. Available: https://ieeexplore.ieee.org/document/10557208

[20] S. Shirvani-Moghaddam and F. Akbari, "A novel ULA-based geometry for improving AOA estimation," *EURASIP J. Adv. Signal Process.*, vol. 2011, no. 1, p. 39, Aug. 2011. [Online]. Available: https://doi.org/10.1186/1687-6180-2011-39

[21] A. Simončič, T. Javornik, A. Sešek, and A. Hrovat, "Direction of arrival estimation for BLE: Antenna array design and evaluation," *AEU Int. J. Electron. Commun.*, vol. 168, Aug. 2023, Art. no. 154722. [Online]. Available: https://www.sciencedirect.com/science/article/pii/S1434841123001966

[22] *VESNA Platform*, Dept. Commun. Syst., Jožef Stefan Inst., Ljubljana, Slovenia, 2013. Accessed: Nov. 14, 2024. [Online]. Available: https://log-a-tec.eu/hw-vesna.html

[23] "AT86RF215 datasheet," Data Sheet, Atmel Corp., San Jose, CA, USA, 2016. Accessed: Nov. 14, 2024. [Online]. Available: https://www.microchip.com/en-us/product/at86rf215

[24] G. Morano, A. Simončič, T. Kocevska, T. Javornik, and A. Hrovat, "Distance- and angle-based hybrid Localization integrated in the IEEE 802.15.4 TSCH communication protocol," *Sensors*, vol. 24, p. 3925, Jun. 2024.

ALEŠ SIMONČIČ (Student Member, IEEE) received the B.Sc. and M.Sc. degrees in electrical engineering from the University of Ljubljana in 2019 and 2022, respectively. He is currently pursuing the Ph.D. degree in information and communication technologies with the Jožef Stefan International Postgraduate School. His master's thesis focused on the estimation of the angle of arrival using BLE technology and antenna arrays. He is currently working as a Young Researcher with the Department of Communication Systems, Jožef Stefan Institute, Ljubljana. His research interests are in radio communication systems, particularly protocols, antennas and arrays, direction of arrival estimation methods, embedded systems, and radio environment characterization.

KE GUAN (Senior Member, IEEE) received the B.E. and Ph.D. degree from Beijing Jiaotong University in 2006 and 2014, respectively.

He is a Full Professor with the State Key Laboratory of Advanced Rail Autonomous Operation and the School of Electronics and Information Engineering, Beijing Jiaotong University. He is with the Department of Communication Systems, Jožef Stefan Institute, Ljubljana, Slovenia. He is the Pole Leader of EURNEX (European Railway Research Network of Excellence). He has authored/coauthored two books and one book chapter, more than 200 journal and conference papers, and four patents. His current research interests include measurements and modeling of wireless propagation channels, high-speed railway communications, vehicle-to-x channel characterization, and indoor channel characterization for high-speed short-range systems, including future terahertz communication systems. In 2015, he has been awarded a Humboldt Research Fellowship for Postdoctoral Researchers. He was the recipient of a 2014 International Union of Radio Science Young Scientist Award. His papers received ten Best Paper Awards, including IEEE Vehicular Technology Society Neal Shepherd Memorial Best Propagation Paper Award in 2019 and 2022. He is an Editor of *IEEE Vehicular Technology Magazine*, IEEE ACCESS, *IET Microwave, Antenna and Propagation*, and *Physical Communication*, and a Guest Editor of the IEEE TRANSACTIONS ON VEHICULAR TECHNOLOGY and *IEEE Communication Magazine*. He serves as the Publicity Chair in PIMRC 2016, the Publicity Co-Chair in ITST 2018, the Track Co-Chair in EuCNC, the International Liaison of EUSIPCO 2019, the Session Convener of EuCAP 2015–2022, and a TPC Member for many IEEE conferences, such as Globecom, ICC, and VTC. He has been a delegate in 3GPP and a member of the IC1004 and CA15104 initiatives.

GREGA MORANO (Graduate Student Member, IEEE) received the M.Sc. degree in electrical engineering from the University of Ljubljana in 2021. He is currently pursuing the Ph.D. degree in information and communication technologies with the Jožef Stefan International Postgraduate School.

He is a Research Assistant with the Department of Communication Systems, Jožef Stefan Institute, Ljubljana. His research interests include IoT communication protocols, integrated sensing and communication, wireless sensor networks, and wireless experimental testbeds.

ALEŠ ŠVIGELJ (Senior Member, IEEE) received the B.Sc., M.Sc., and Ph.D. degrees in electrical engineering from the University of Ljubljana, Ljubljana, Slovenia, in 1997, 2000, and 2003 respectively.

He is a Senior Research Fellow with the Department of Communication Systems, Jožef Stefan Institute and a Full Professor with the Jožef Stefan Postgraduate School. He has extensive research in modeling, simulation, and design of advanced telecommunications elements, systems, and services. He has also participated as a coordinator in several national and international projects, including COST Projects. He co-authored several books/book chapters and more than 100 peer-reviewed journal and conference papers. His current work focuses on advanced networking technologies for wireless systems.

ANDREJ HROVAT (Senior Member, IEEE) received the B.Sc. and M.Sc. degrees in electrical engineering from the University of Ljubljana in 2004 and 2008, respectively, and the Ph.D. degree from the Jozef Stefan International Postgraduate School in 2011.

He has been with the Department of Communication Systems, Jožef Stefan Institute since 2004, where he is currently a Senior Research Fellow. He is the author or a co-author of more than 120 peer-reviewed journal and conference papers. He works on several projects connected with professional mobile communication systems, 2G-5G, WiFi and IoT technologies, satellite and sensor networks, including several COST actions, Framework Program projects, H2020 projects, European Space Agency projects, and numerous national research and application projects. His research and working experience are in telecommunications, focusing on development and performance analysis for fixed and mobile systems, including terrestrial, stratospheric, and satellite systems, and radio-channel modeling for fixed and mobile narrowband and broadband radio communication systems. He serves as a journal editorial board member and a guest editor, is a reviewer for several international impact-factor journals, and is a TCP member for various international conferences and workshops.

TEODORA KOCEVSKA (Member, IEEE) received the B.Sc. and M.Sc. degrees in electrical engineering from the Ss. Cyril and Methodius University, Skopje, North Macedonia, in 2017 and 2018, respectively, and the Ph.D. degree from the Jožef Stefan International Postgraduate School, Ljubljana, Slovenia, in 2023.

She has been with the Department of Communication Systems, Jožef Stefan Institute since 2019, where she is currently a Research Assistant. Her research experience is in telecommunications, focusing on radio channels, integrated communications and sensing, radio environment characterization, environmentally aware communications, and the application of machine learning in telecommunications.

TOMAŽ JAVORNIK (Member, IEEE) received the B.Sc., M.Sc., and Ph.D. degrees in electrical engineering from the University of Ljubljana, Ljubljana, Slovenia, in 1987, 1990, and 1993, respectively. He is a Scientific Counsellor with the Communication Systems Department, Jozef Stefan Institute, Ljubljana, and an Assistant Professor with the Jozef Stefan International Postgraduate School, Ljubljana. He participated in several COST and Framework Programme projects. He has co-authored more than 100 refereed journal and conference papers and several books and book chapters in mobile and wireless communications. He holds two international patents. His research experience is in telecommunications, focusing on the development and performance analysis of fixed and mobile systems, radio-channel measurements, modeling and simulations, and indoor localization. He serves as a TPC member or a reviewer for several IEEE conferences and journals.